

Long-Lived Oscillons as Closed Domain Walls in the \mathbb{Z}_2 -Symmetric Two-Higgs-Doublet Model

Zhaoyu Meng

JAN 2026

Abstract

We identify an oscillatory solution that exists as a long-lived, bubble-like closed domain wall in the two-Higgs-doublet model (2HDM) under a \mathbb{Z}_2 symmetry constraint, and these structures emerge naturally during the late stages of domain wall decay.

The longevity of these structures is attributed to a potential landscape characterized by two distinct vacuum regions, the oscillating region lies in one vacuum, while the constant outer region lies in the other. The lifetime of the structure depends on the parameter in the Lagrangian, we identify a specific parameter space where radiation is suppressed, the solution exhibits a maximum lifetime that goes up to infinity.

The simpler two-complex-field system is first used to introduce the mathematical requirements of the structure before extending it to the more physical but complex 2HDM. Further Numerical verification via Floquet analysis shows these structures are stable under perturbation.

CONTENTS

I. Introduction	2
II. \mathbb{Z}_2 -symmetry 2-Higgs Doublet Model	3
III. Phenomenology and Computer Analysis	5
A. System Setup	5
B. Late-time Evolution of Domain Wall Decay	6
C. Natural Forming Rate	8
IV. Reconstruct the Radiation-free structure with two complex scalar fields	9
A. Oscillon Solution	9
B. Stability of the Structure	14
C. Full expansion of theory in \mathbb{Z}_2 -2HDM	15
V. Conclusion	18
Acknowledgments	18
References	18
Appendix 1: 2HDM mass and parameters	20
Appendix 2: parameter and mass in 4-field system	21
Appendix 3: Floquet Analysis	23

I. INTRODUCTION

Topological defects form during spontaneous symmetry breaking when fields in different regions of space independently fall into one of the distinguishable vacuum minimum states, when the system gradually cools down from the Big Bang [1–3]. When the early universe gradually cools from such a hot, dense, homogeneous, isotropic initial state, defects like cosmic strings and domain walls can form [4–7], where their structures are the key to investigating how the universe evolved during its earliest period [5].

Domain wall is an important topological concept and could lead to various cosmological phenomena in the early universe, such as the Primordial black hole [8]. There are various types of domain walls [7], and this paper focuses on the wall arise from \mathbb{Z}_2 symmetry.

Based on previous findings of the domain wall evolution in \mathbb{Z}_2 2HDM [4], studies have established that domain walls typically collapse in an increasing rate after formation, in general parameter choices. However, in our realization, we show that at the end of the decay, the decay rate diverges from the previous prediction, and becomes a long-lived, closed localized domain wall.

This anomalous longevity necessitates a detailed investigation into the underlying stabilizing mechanisms. Some models have been proposed to explain a closed stable domain wall, and there have been discussions over biased vacuum [9] and others regarding kinky Vortons [10, 11]. However, in our phenomena observation in 2HDM, a stable closed domain wall structure (which we will call it "bubble" in the following discussion) with an abnormally long lifetime was observed in the \mathbb{Z}_2 -2HDM at the end of closed-domain-wall decay. We found the structure exists under a symmetric degenerated vacuum, and it exhibits a perfect spherical wall in 3-dimensional space. This means it is excluded from the scenario of biased vacuum, and it is not likely to be supported by kinky Vortons' angular momentum, otherwise the structure shape will be a disk.

Unlike conventional oscillons derived from small-field expansions, the structures identified here are large-amplitude configurations interpolating between two degenerate vacua, effectively forming a self-trapped spherical domain wall. Our goal is to give a new mathematical structure to characterize the long-lived bubble-like structures observed, and to correlate the derivation in the decay curve. We also would like to determine some properties of its mathematical structure, and compare them with some classical oscillatory models.

II. \mathbb{Z}_2 -SYMMETRY 2-HIGGS DOUBLET MODEL

The 2-Higgs Doublet Model (2HDM) is a Beyond the Standard Model theory that combines two Higgs fields as a whole [4]. Compared to the single Higgs model which is constructed by two complex scalar fields, the 2HDM is composed of two complex doublets. 2HDM exhibits the Standard Model symmetries of $SU(2) \otimes U(1)$ as the single Higgs field does [12, 13], but the additional field involved allows the 2HDM to have more geometric characteristics due to the increased complexity of the vacuum manifold's homotopy group [12–14]. By introducing the new properties as extensions to the basic Standard Model symmetry, 2HDM potentially offers new insights into unresolved questions in Standard Model and early universe physics areas, like supersymmetry [15], CP-violation [16], and dark matter [17].

Apart from basic Standard Model symmetries, some additional constraints can also be applied to the 2HDM [18]. \mathbb{Z}_2 symmetry is one of the most commonly used constraints that allows the domain walls of the topological defects to be produced when applied [4, 13, 18]. Additionally, compared to alternative constraints such as CP1 and CP2 symmetries, \mathbb{Z}_2 symmetry makes both disjoint vacuum manifolds lie in the real space regime [13, 18]. In the \mathbb{Z}_2 -2HDM, both the potential and kinetic parts of the Lagrangian are invariant under the transformation of $\Psi_1 \rightarrow \Psi_1$ and $\Psi_2 \rightarrow -\Psi_2$, for Ψ_1 and Ψ_2 are two complex scalar fields doublet in the 2HDM [4]. For 2HDM to exhibit such symmetry, some constraints need to be applied to the potential part of the Lagrangian [4, 10, 19], where the Lagrangian under such constraint is [4, 10]

$$\mathcal{L} \supset (\partial_\mu \Psi_1)^\dagger (\partial^\mu \Psi_1) + (\partial_\mu \Psi_2)^\dagger (\partial^\mu \Psi_2) - V(\Psi_1, \Psi_2), \quad (2.1)$$

however, QCD effects are beyond the scope of this work. The potential part of the Lagrangian is given by [10, 13, 19].

$$\begin{aligned} V(\Psi_1, \Psi_2) = & -\mu_1^2(\Psi_1^\dagger \Psi_1) - \mu_2^2(\Psi_2^\dagger \Psi_2) + \lambda_1(\Psi_1^\dagger \Psi_1)^2 + \lambda_2(\Psi_2^\dagger \Psi_2)^2 + \lambda_3(\Psi_1^\dagger \Psi_1)(\Psi_2^\dagger \Psi_2) \\ & + (\lambda_4 - |\lambda_5|) \left[\text{Re}(\Psi_1^\dagger \Psi_2) \right]^2 + (\lambda_4 + |\lambda_5|) \left[\text{Im}(\Psi_1^\dagger \Psi_2) \right]^2, \end{aligned} \quad (2.2)$$

and under such \mathbb{Z}_2 , we may introduce a parameter R^1 to distinguish two vacuum manifolds, where the expression is given by [10, 13, 19]

$$R^1 = \Psi_1^\dagger \Psi_2 + \Psi_2^\dagger \Psi_1, \quad (2.3)$$

where positive and negative signs of R^1 represent two distinct manifolds, and $R^1 = 0$ is the boundary between the two regions, which is called the domain wall. [18].

In the detailed analysis and plotting of two complex doublet fields in the 2HDM system, we may break and decompose the system into 8 independent scalar fields. Fields in the 2-Higgs Doublet Models can be expressed as the combination of 8 scalar fields [18]:

$$\Psi_1 = \begin{pmatrix} \psi_1 + i\psi_3 \\ \psi_5 + i\psi_7 \end{pmatrix}, \quad \Psi_2 = \begin{pmatrix} \psi_2 + i\psi_4 \\ \psi_6 + i\psi_8 \end{pmatrix}, \quad (2.4)$$

which can be used to expand the potential parts of the 2HDM Lagrangian as [18]

$$\begin{aligned} V = & -\mu_1(\psi_1^2 + \psi_3^2 + \psi_5^2 + \psi_7^2) - \mu_2(\psi_2^2 + \psi_4^2 + \psi_6^2 + \psi_8^2) + \lambda_1(\psi_1^2 + \psi_3^2 + \psi_5^2 + \psi_7^2)^2 \\ & + \lambda_2(\psi_2^2 + \psi_4^2 + \psi_6^2 + \psi_8^2)^2 + \lambda_3(\psi_1^2 + \psi_3^2 + \psi_5^2 + \psi_7^2)(\psi_2^2 + \psi_4^2 + \psi_6^2 + \psi_8^2) \\ & + (\lambda_4 - |\lambda_5|)(\psi_1\psi_2 + \psi_3\psi_4 + \psi_5\psi_6 + \psi_7\psi_8)^2 + (\lambda_4 + |\lambda_5|)(\psi_1\psi_4 - \psi_3\psi_2 + \psi_5\psi_8 - \psi_7\psi_6)^2, \end{aligned} \quad (2.5)$$

and the equations of motion for each of the ψ_i are therefore given by [18]:

$$\begin{aligned}
\ddot{\psi}_{1,3,5,7} = & \nabla^2 \psi_{1,3,5,7} + \mu_1 \psi_{1,3,5,7} \\
& - 2\lambda_1 \psi_{1,3,5,7} (\psi_1^2 + \psi_3^2 + \psi_5^2 + \psi_7^2) - \lambda_3 \psi_{1,3,5,7} (\psi_2^2 + \psi_4^2 + \psi_6^2 + \psi_8^2) \\
& - (\lambda_4 - |\lambda_5|) \psi_{2,4,6,8} (\psi_1 \psi_2 + \psi_3 \psi_4 + \psi_5 \psi_6 + \psi_7 \psi_8) \\
& - (\lambda_4 + |\lambda_5|) \psi_{4,8,-2,-6} (\psi_1 \psi_4 - \psi_3 \psi_2 + \psi_5 \psi_8 - \psi_7 \psi_6),
\end{aligned} \tag{2.6}$$

$$\begin{aligned}
\ddot{\psi}_{2,4,6,8} = & \nabla^2 \psi_{2,4,6,8} + \mu_2 \psi_{2,4,6,8} \\
& - 2\lambda_2 \psi_{2,4,6,8} (\psi_2^2 + \psi_4^2 + \psi_6^2 + \psi_8^2) - \lambda_3 \psi_{2,4,6,8} (\psi_1^2 + \psi_3^2 + \psi_5^2 + \psi_7^2) \\
& - (\lambda_4 - |\lambda_5|) \psi_{1,3,5,7} (\psi_1 \psi_2 + \psi_3 \psi_4 + \psi_5 \psi_6 + \psi_7 \psi_8) \\
& - (\lambda_4 + |\lambda_5|) \psi_{-3,-7,1,5} (\psi_1 \psi_4 - \psi_3 \psi_2 + \psi_5 \psi_8 - \psi_7 \psi_6),
\end{aligned} \tag{2.7}$$

with introduce notation of $\psi_{-i} = -\psi_i$.

To investigate the 2HDM, one may try to approach it from simplified models that contain fewer degrees of freedom, but the same fundamental characteristics. For such systems with these simplified field models, we may replace Ψ_1, Ψ_2 in the equations of motion with real scalar fields or complex scalar fields, corresponding to the 2-fields model, the 4-fields model. Using the 2-field model and 4-field model provides a simplified approach to 2HDM dynamics, as they involve a smaller number of evolving fields, making computation easier [10]. And using the difference between analyzing results between those systems, to understand the effects of additional mechanics from extra dimensions.

III. PHENOMENOLOGY AND COMPUTER ANALYSIS

A. System Setup

By discretizing space into a grid, one can calculate the first and second derivative values of grids by the values of the fields of a point and its neighborhood. With parameters given in Appendix 1, All grids are iterated in each time interval concurrently via the equation of motion given by equations (2.6) and (2.7) in the previous part, for time to progress in the system. We use the RK4 method in calculating our spatial derivative terms.

If the system has random initial conditions, each grid's initial field value is set with random numbers that are uniformly distributed between -1 and +1, to simulate an early hot, dense, homogeneous universe and how it evolves when it starts to cool down [10]. A friction term is added to the system during the initial iteration steps to simulate cooling [10]. We may also apply continuous boundary conditions, which set in a way that the system is wrapped as a torus, by joining one side to its opposite. But we should be aware

that such boundary conditions may cause some nonphysical wrapping strip mode [10] and they need to be neglected in physical analysis.

Periodic boundary conditions, which permit outgoing particles (or waves) to re-enter the computational domain from the opposite side, can be suitable for modeling the early radiation-dense universe with highly frequent random collisions. However, they are inadequate for systems that require an asymptotically vacuum state at infinity.

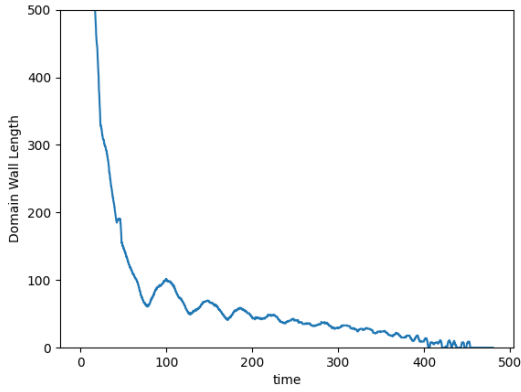
If we require approximating the infinite, non-reflecting exterior, we should replace the periodic boundaries with the sponge-layer absorbing boundary condition [20], where an artificial damping term is added to the equations of motion in a boundary region, with higher damping when it's farther. Compared to other absorbing boundary conditions like Mur-ABC [21], this method does not require us to know the wave-speed, and our system has various vibration modes from the mass spectrum, as shown in Appendix 2. We also set the boundary in a circular shape to minimize any potential impact of oblique incidence.

B. Late-time Evolution of Domain Wall Decay

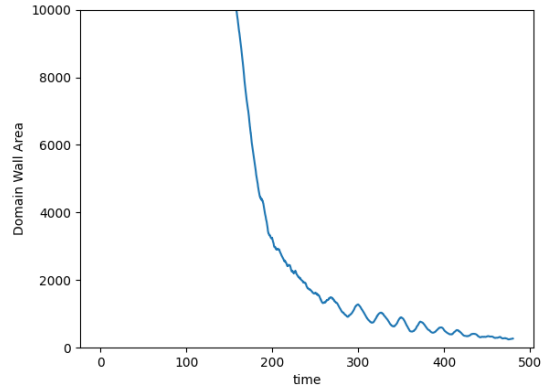
For the domain wall arising from Spontaneous symmetry breaking in the early universe, we use random initial conditions and periodic boundary conditions to set up the system and observe how the structure of the wall changes when iterating in time.

After the damping period in forcing the system to cool down, the domain wall will tend to contract to minimize its length as the wall has a higher energy density than the vacuum in the Higgs field. Simulations show that the size of the domain wall structure (circumference) maintained non-zero values for the domain wall length for extended periods before ultimately collapsing into a single domain. These were found to be circular, bubble-like structures that decay much more slowly than other parts of the structure in the space.

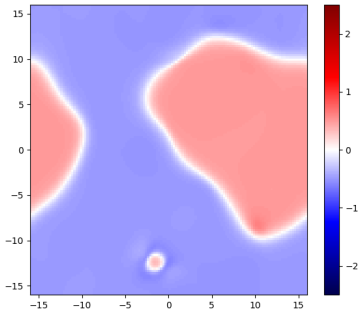
As shown in FIG. 1, after approximately $t = 50.0$ in 2D and $t = 250.0$ in 3D, the decay rate is significantly slower than the early stage prediction [4]. The system is set up with random initial conditions and periodic boundary conditions (toroidal space) [10], however, the periodic boundary condition gives that the radiating background particle(stochastic perturbations) may re-enter system from the other side, the structure is immersed in a high-density collision condition, and the lifetime of the structure is highly reduced compared to what it could be in clean space.



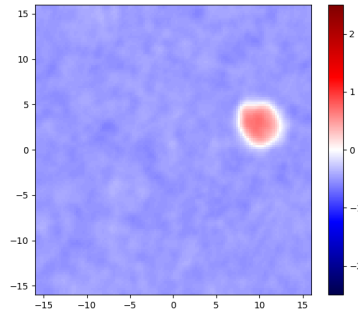
(a)



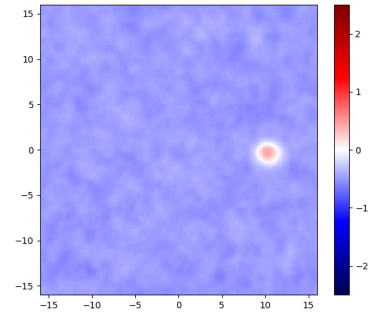
(b)



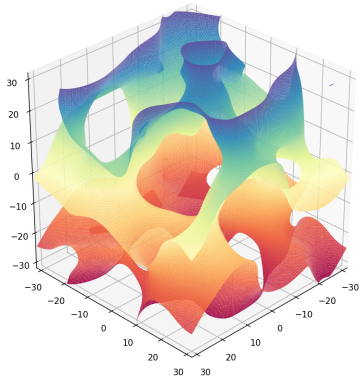
(c)



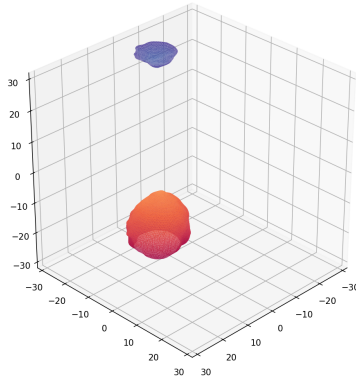
(d)



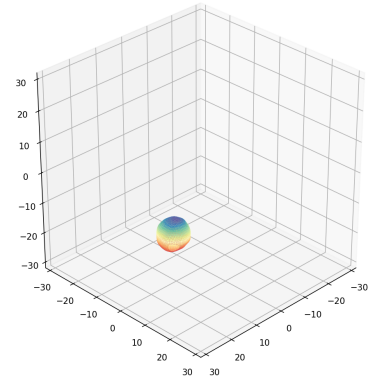
(e)



(f)



(g)



(h)

FIG. 1. Plot of how domain wall length(area) change in time, in 2D(a) and 3D(b) space. (c-e) and (f-h) show the plot of the domain wall structure at the timeslice 40(c,f), 240(d,g), 360(e,h).

2D graphs plot the R^1 distribution with values, while 3D plots only illustrate surface where $R^1 = 0$. The departure from the earlier period decay rate signals the formation of stable oscillon relics. The diameter of Bubbles in 3D was measured to be the same from different directions.

2D example shown in FIG. 1 will be used in the following simulations, as 3D analysis will take too long to run due to the complexity from the extra dimension in grid space. Result from FIG. 1 shows they have a similar pattern in producing long-lived closed domain wall so they should share the same mechanics.

C. Natural Forming Rate

We would then like to know if such a phenomenon exists in 2HDM only or in any \mathbb{Z}_2 -symmetry model in general. We would like to try to plot the terminal period of the decay curve in different models, in searching for the conditions required for such a structure to be produced.

In the introduction of 2-fields and 4-fields, as a comparison with 8-fields 2HDM in investigating the mechanics of the long-lived structure, and compare to complex doublet Ψ_1, Ψ_2 in 2HDM Lagrangian, we replace Ψ_1, Ψ_2 with two real scalar fields or two complex scalar fields ¹ in representing 2-fields or 4-fields systems. In such cases, we only preserve ψ_1 and ψ_2 , or ψ_1 to ψ_4 valid, and remove all other fields in the equation (2.6) and (2.7).

For each field model (2-fields, 4-fields, 2HDM), we conducted extensive numerical surveys comprising hundreds of independent trials. As we are only interested in the physical abnormal curve at the end of decay, we should only consider trials that end in single domain [10] final states(all in one vacuum) only.

We define 'lifetime'(bubble period), that start from when the domain wall length first falls below the minimum required to form a stripe in space [10], and ends at the wall length reaching zero for the first time. We neglect all trials with "lifetime" undefined to ensure that stripe modes are excluded. Therefore, in all three modes, the 'lifetime' of each trial of simulation is plotted in a histogram of probability density against lifetime as shown in FIG. 2.

Previous research predicts that general systems are decaying at an increasing but certain rate [10], and the existence of bubbles can greatly slow down the decay to extend the lifetime of the structure, as shown in FIG. 1. Hence, the more the histogram plot spreads out, the more bubbles are expected to exist, as the system is more divergent from the certain decay rate prediction. Therefore, FIG. 2 shows a lot of long-lived bubbles in 2HDM, fewer natural bubbles in the 4-fields model, and no (or very few) natural bubbles in the 2-fields model.

¹ Two complex scalar fields is identical to two scalar doublet, so only one of those is use for plot.

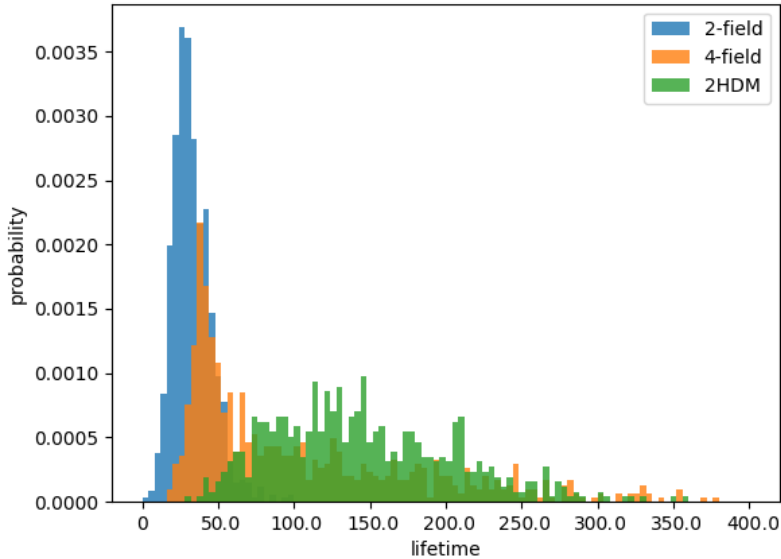


FIG. 2. Histogram of plot of ‘lifetime’ in 2-fields, 4-fields, 2HDM for comparison. Parameters used were given in Appendix 2. The probability is measured by the chance of falling in each bin, with the bin width is 40.

The numerical results in FIG. 2 indicates that the 4-field model, while producing fewer long-lived bubbles than the full 2HDM, still exhibits the phenomenon. This suggests that the 4-field model represents the minimal theoretical framework capable of sustaining such oscillatory solutions, and the topological structure of the 4-field model can be embedded into 2HDM automatically, which means the 4-field model can be used as a simpler substitute for 2HDM in functional analysis.

IV. RECONSTRUCT THE RADIATION-FREE STRUCTURE WITH TWO COMPLEX SCALAR FIELDS

A. Oscillon Solution

Now let us consider the minimal model that accommodates an oscillon, 4-field system, expressed in terms of two complex scalars Ψ_1 and Ψ_2 . In searching for a system that can maximize the structure lifetime, we identify a specific parameter subspace where high-order terms responsible for radiation are suppressed [22, 23]. Under such conditions, parameters in the Lagrangian should satisfy:

$$\begin{aligned}
\mathcal{L} &= (\partial_\mu \Psi_1)^2 + (\partial_\mu \Psi_2)^2 - V(\Psi_1, \Psi_2) \\
V(\Psi_1, \Psi_2) &= -\mu^2(\Psi_1^\dagger \Psi_1) - \mu^2(\Psi_2^\dagger \Psi_2) + \lambda(\Psi_1^\dagger \Psi_1)^2 + \lambda(\Psi_2^\dagger \Psi_2)^2 + 2\lambda(\Psi_1^\dagger \Psi_1)(\Psi_2^\dagger \Psi_2) \\
&\quad + 2\lambda_4 \left[\text{Re}(\Psi_1^\dagger \Psi_2) \right]^2,
\end{aligned} \tag{4.1}$$

Turning off λ_4 , the potential is then enhanced to be $SU(2)$ -invariant with $\Psi = (\Psi_1, \Psi_2)^T$ the doublet. But we need $\lambda_4 \neq 0$ where reasons given in Appendix 2.

We may decompose the two complex fields Ψ_1 and Ψ_2 in terms of the real and imaginary parts, that $\Psi_1 = \psi_1 + i\psi_2$ and $\Psi_2 = \psi_3 + i\psi_4$, where the simplest solution that gives a stable Exact Oscillon solution is in the form of

$$\begin{aligned}
\psi_1 &= +f_0 \cos(\alpha) + f_1 \cos(\omega t), & \psi_2 &= -f_0 \sin(\alpha) - f_1 \sin(\omega t), \\
\psi_3 &= -f_0 \cos(\alpha) + f_1 \cos(\omega t), & \psi_4 &= +f_0 \sin(\alpha) - f_1 \sin(\omega t),
\end{aligned} \tag{4.2}$$

for four scalar fields ψ_i and α is an arbitrary phase constant that reflects continuous vacuum degeneracy and does not affect the oscillon profile. And we expect when there are no higher-order terms ($\cos(2\omega t)$, $\cos(3\omega t)$, ect) up to infinity, there will be no radiation [22, 23].

The equation of motion can be rearranged by substituting terms in forms of f_0 and f_1 terms, hence we may obtain

$$\begin{aligned}
0 &= -\frac{d^2}{dt^2}(f_0 \cos(\alpha) + f_1 \cos(\omega t)) + \nabla^2(f_0 \cos(\alpha) + f_1 \cos(\omega t)) + \mu(f_0 \cos(\alpha) + f_1 \cos(\omega t)) \\
&\quad - 2\lambda(f_0 \cos(\alpha) + f_1 \cos(\omega t))((f_0 \cos(\alpha) + f_1 \cos(\omega t))^2 + (-f_0 \sin(\alpha) - f_1 \sin(\omega t))^2) \\
&\quad - 2\lambda(f_0 \cos(\alpha) + f_1 \cos(\omega t))((-f_0 \cos(\alpha) + f_1 \cos(\omega t))^2 + (f_0 \sin(\alpha) - f_1 \sin(\omega t))^2) \\
&\quad - 2\lambda_4(-f_0 \cos(\alpha) + f_1 \cos(\omega t))(f_0 \cos(\alpha) + f_1 \cos(\omega t))(-f_0 \cos(\alpha) + f_1 \cos(\omega t)) \\
&\quad - 2\lambda_4(-f_0 \cos(\alpha) + f_1 \cos(\omega t))(-f_0 \sin(\alpha) - f_1 \sin(\omega t))(f_0 \sin(\alpha) - f_1 \sin(\omega t)),
\end{aligned} \tag{4.3}$$

For the equation of motion of ψ_1 as an example.

Under this specific parameterization, the source terms for third and higher-order harmonics cancel exactly through trigonometric identities. Consequently, the equations of motion for the four-field system reduce to a closed set of coupled differential equations for the base frequency components f_0 and f_1 .

$$\begin{aligned}
0 &= -\frac{d^2}{dt^2}(f_0 \cos(\alpha) + f_1 \cos(\omega t)) + \nabla^2(f_0 \cos(\alpha) + f_1 \cos(\omega t)) + \mu(f_0 \cos(\alpha) + f_1 \cos(\omega t)) \\
&\quad - 2\lambda(f_0 \cos(\alpha) + f_1 \cos(\omega t))(2f_0^2 + 2f_1^2) - 2\lambda_4(-f_0 \cos(\alpha) + f_1 \cos(\omega t))(-f_0^2 + f_1^2),
\end{aligned} \tag{4.4}$$

which can be decomposed based on the frequency spectrum($\cos(\alpha)$ and $\cos(\omega t)$), the functions of f_1 and f_2 should satisfy

$$0 = \nabla^2 f_0 + \mu^2 f_0 - (4\lambda + 2\lambda_4) f_0^3 - (4\lambda - 2\lambda_4) f_0 f_1^2, \quad (4.5)$$

$$0 = \omega^2 f_1 + \nabla^2 f_1 + \mu^2 f_1 - (4\lambda + 2\lambda_4) f_1^3 - (4\lambda - 2\lambda_4) f_1 f_0^2. \quad (4.6)$$

and starting from the equation of motion of the other 3 fields will all end with the same result.

Consider the boundary effects at infinity, we may also expect f_0 and f_1 follow that, when $r \rightarrow \infty$, $f_1 = 0$, and $f_0 = \sqrt{\frac{\mu^2}{4\lambda+2\lambda_4}}$ is the vacuum value, as well as $\nabla f_1 = \nabla f_2 = 0$. After applying those boundary conditions, shape of the functions are plotted in FIG. 3.

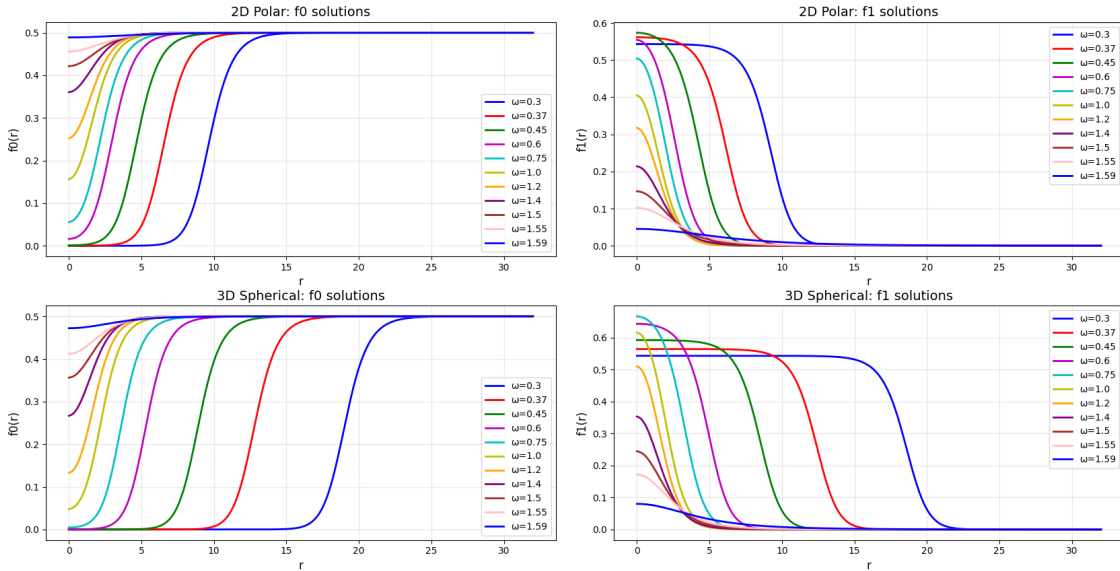


FIG. 3. Plot of f_0 and f_1 in 2D and 3D space, with choice of parameter $\mu = 0.5$, $\lambda = 1.78$, and $\lambda_4 = -2.56$ as in Appendix 2. When frequency is low, the oscillation has high amplitude and the system lies in the opposite vacuum manifold than the constant outer region. When the angular frequency ω is high, the system becomes a small-amplitude oscillation, there is no crossing of the domain wall, and all regions stay in the same vacuum. There is a maximum frequency $\omega_m = 1.6$ where any system should have a frequency below that $\omega < \omega_m$. Solutions were found based on the Newton-Raphson method via Python ‘fslolve’ code.

We numerically find the oscillon configurations and demonstrate them in FIG. 3. The profiles of the oscillon depend on ω :

- The maximum frequency of the system, ω_m , also have relationship, that $m_H^2 = V''(\text{vacuum}) = \mu^2 \frac{2|\lambda_4|}{2\lambda + \lambda_4} = 2.56 = \omega_m^2$, with m_H is the mass term of the system given in Appendix 2. As ω approach to ω_m , the functions are having smaller amplitude with a wider peak, getting closer to horizontal lines(vacuum).
- One type is domain wall like for the low ω : the center of the oscillon is near one vacuum with $f_0(0)$ almost vanishes while $f_1(0)$ approaches v ; $f_0(r)$ and $f_1(r)$ grow and decrease towards the outer region, respectively, interpolating in another vacuum. One may notice that, for small ω , there is an obvious flat-top structure (with $\nabla^2 f_1(r) \approx 0$) with certain width within which $f_0(r) \rightarrow 0$ and the oscillating amplitude keeps constant

$$f_1^2(r) \approx \frac{\mu^2 - \omega^2}{2(2\lambda + \lambda_4)}. \quad (4.7)$$

Thus, the width narrows as the frequency increases; at the same time, the oscillating amplitude $f_1(r)$ increases.

- As ω increases to some critical value $\omega_c = \sqrt{\mu^2}$, the flat-top vanishes and turns into the Gaussian peak.
- As we increases ω and $\omega \rightarrow \omega_c$, the width of the Gaussian peak extends, but the height(oscillating amplitude) shrinks. The corresponding solutions are not domain wall-like, because the fields are just oscillating slightly around one vacuum, which is called a small-amplitude oscillation.
- As $\omega \rightarrow 0$, the inner region of the opposite vacuum goes infinitely large, and that space fully goes into the opposite vacuum. This indicates that the nature of this structure is indeed a closed-wall separating two vacuum shown in FIG. 1, and a large-scale closed-domain wall structure is possible to exist without decay in cosmology.

After successfully obtaining the mathematical expression of the structure, we try to reproduce this in the lattice grid simulation. Different from the previous background dense periodic boundary conditions for simulate early universe, we try the sponge-layer absorbing boundary condition [20] to absorb any possible radiation to ensure the structure is in a clean space. As shown in FIG. 4, fields involved in the simulation are made in a purely circular symmetrical pattern, which means that the bubbles can exist without any circular motion. We found the field distribution in the simulation shown in FIG. 4 is exactly the same as predicted by the previous analysis.

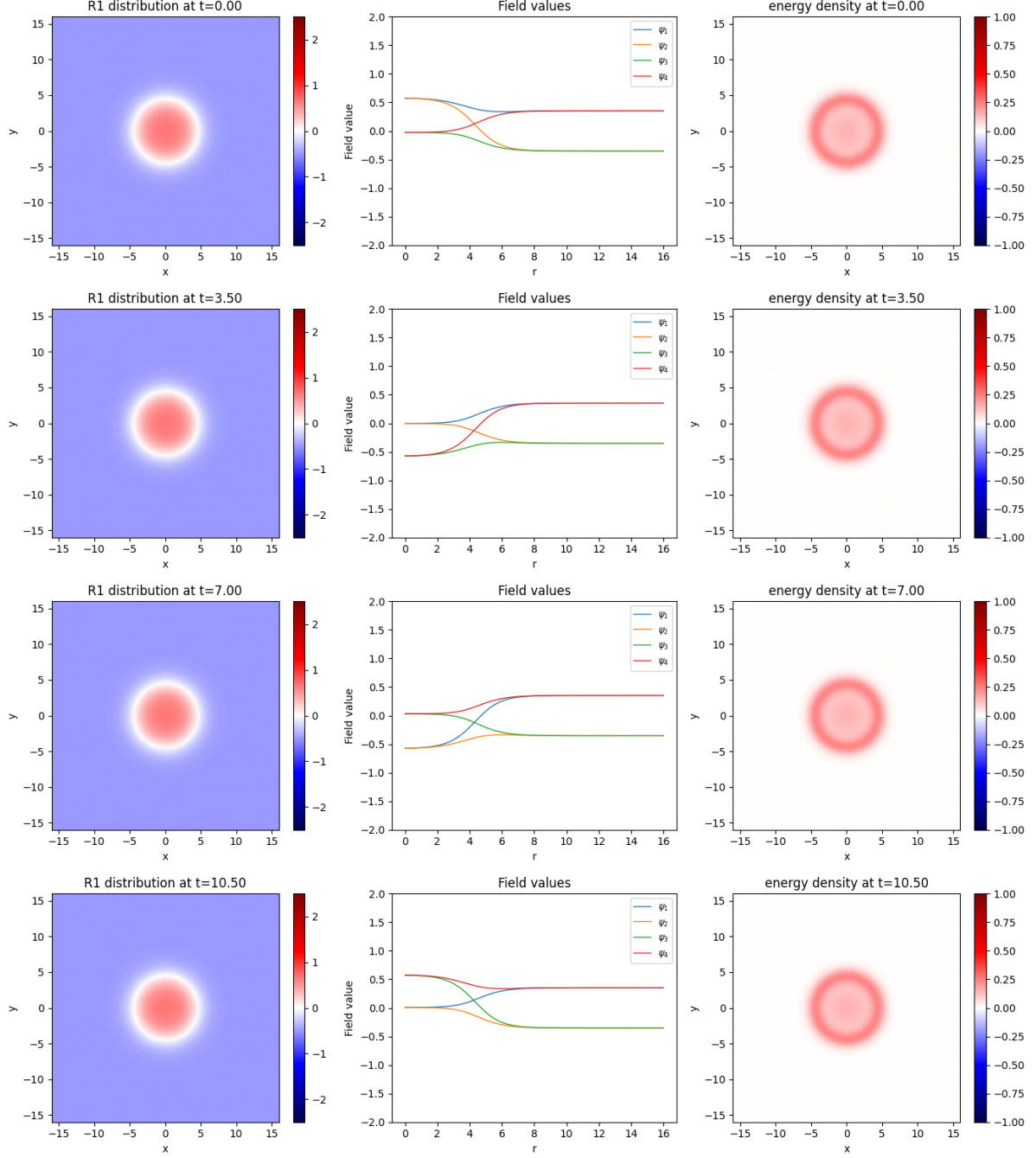


FIG. 4. The plot of time slice at rotating phase of fields in $0, \pi/2, \pi, 3\pi/2$. with the R^1 distribution (left column), radial field distribution (middle column), and energy distribution (right column) plot. The plot use constant phase $\alpha = \pi/4$, and other parameters used are from Appendix 2 with full mixing. The sponge-layer absorbing boundary condition is used to replace periodic ones.

B. Stability of the Structure

We would like to check if the system is stable or not under perturbation, in a way determine if the structure will diverge from the solution over time. In the case when the system evolves in a periodic oscillation, we would like to introduce the Floquet analysis method, which compares the perturbation scale change after a complete cycle of oscillation. An oscillon solution requires that the perturbation should not expand over time.

For the mechanics of Floquet analysis discussed in Appendix 3, and for $\omega = 0.45$ curve in FIG. 3 as an example ², Floquet analysis in circular symmetry perturbation modes gives the result: some mode gives eigenvalues smaller than or equal to (with less than $\pm 10^{-16}$ uncertainty) 1, as shown in FIG. 5, indicating the system will become stable against first-order small-scale perturbations over time.

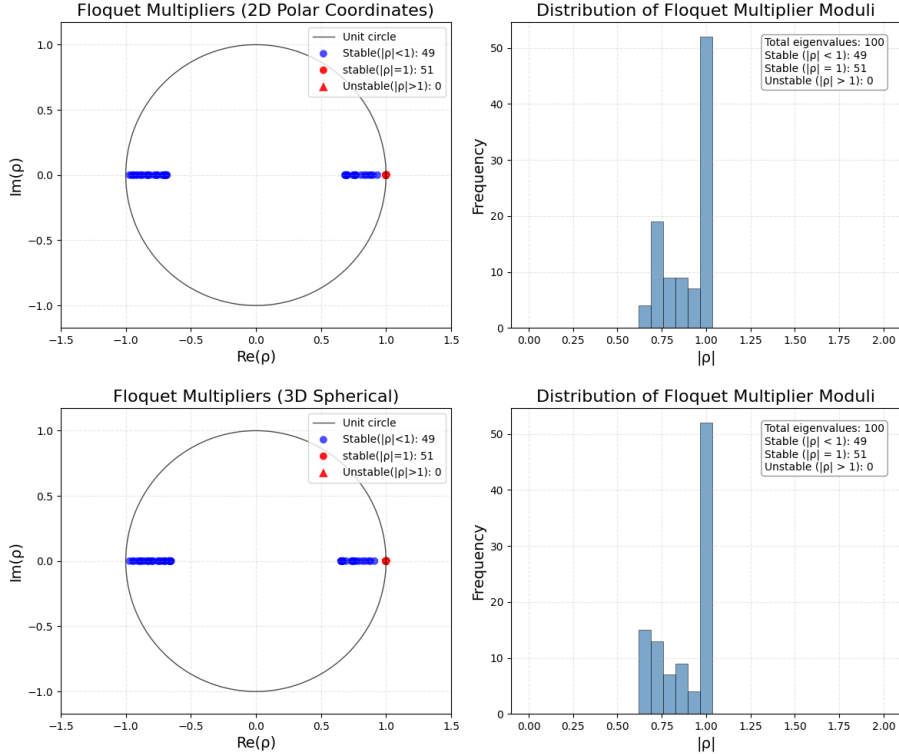


FIG. 5. 100 random chosen eigenvalues from the matrix of Floquet analysis. 'equal to 1' include values within 1 ± 10^{-5} due to the consideration of decimal uncertainties from grids and iteration(though output range can narrow to 1 ± 10^{-15}). parameters and background are chosen from FIG. 3 with $\omega = 0.45$.

² We have also tried to analyze the stability from some other setup mode, like all other plots with different frequencies in FIG. 3, their analysis results are all stable. And they give the same distribution in the plot.

Floquet analysis in FIG. 5 shows that there are no modes that expand over time in radial perturbation; the system is stable in radial modes. Under non-radial perturbation modes, from which perturbation is decomposed into a summation of modes with different angular spectrum $\delta(t, r, \theta) = \sum_l \delta_l(t, r) e^{il\theta}$, where each of term in them gives a shift to the potential by

$$V_{eff}(r, l) = V(r) + l^2/r^2 \quad (2D), \quad V_{eff}(r, l) = V(r) + l(l+1)/r^2 \quad (3D). \quad (4.8)$$

For all $\partial^2 \delta / \partial t^2 = [\nabla^2 - V_{eff}(r, l)] \delta$ where there is $V_{eff}(r, l) > V(r)$ at $l \geq 1$, these non-radial modes are energetically more confined than the radial ($l = 0$) mode. Since the radial modes are already proven stable (as shown in FIG. 5), the system is consequently stable against perturbations in any angular momentum sectors.

C. Full expansion of theory in \mathbb{Z}_2 -2HDM

While the 4-field subsystem provides the minimal framework for non-radiating oscillons, it is imperative to verify if these configurations remain viable within the full structure of the 2HDM. We therefore map the previous ansatz onto the eight-field field space of the full complex doublet potential, to ensure the cancellation of high-frequency terms.

We use a set of parameter values from Appendix 1 [4, 13, 24], but modifying the mixing parameter to $a = b = \pi/4$ to satisfy the cancellation condition. Then, parameters in the Lagrangian can be rearrange into [4, 10]

$$V(\Psi_1, \Psi_2) = -\mu^2(\Psi_1^\dagger \Psi_1) - \mu^2(\Psi_2^\dagger \Psi_2) + \lambda(\Psi_1^\dagger \Psi_1)^2 + \lambda(\Psi_2^\dagger \Psi_2)^2 + 2\lambda(\Psi_1^\dagger \Psi_1)(\Psi_2^\dagger \Psi_2) + 2\lambda_4 \left[\text{Re}(\Psi_1^\dagger \Psi_2) \right]^2 + 0 \left[\text{Im}(\Psi_1^\dagger \Psi_2) \right]^2, \quad (4.9)$$

with $\mu^2 = 0.5$, $\lambda = 1.78$, and $\lambda_4 = -2.56$, the higher frequency terms $\cos^2(\omega t)$ and $\sin^2(\omega t)$ vanish in the same way as in the 4-field system discussed in the 4-field section. Those values will be used in the rest of the research.

Like the solution in the 4-field system, the two complex fields doublet of the 2HDM,

$$\Psi_1 = \begin{pmatrix} \psi_1 + i\psi_3 \\ \psi_5 + i\psi_7 \end{pmatrix}, \quad \Psi_2 = \begin{pmatrix} \psi_2 + i\psi_4 \\ \psi_6 + i\psi_8 \end{pmatrix}, \quad (4.10)$$

can be expanded in the form of f_1 and f_2 to fit the solution of oscillon

$$\begin{aligned} \psi_1 &= +f_0 \cos(\alpha) + f_1 \cos(\omega t), & \psi_2 &= -f_0 \cos(\alpha) + f_1 \cos(\omega t), \\ \psi_3 &= -f_0 \sin(\alpha) - f_1 \sin(\omega t), & \psi_4 &= +f_0 \sin(\alpha) - f_1 \sin(\omega t), \\ \psi_5 &= +f_0 \cos(\beta) - f_1 \cos(\omega t + \theta_\beta), & \psi_6 &= -f_0 \cos(\beta) - f_1 \cos(\omega t + \theta_\beta), \\ \psi_7 &= +f_0 \sin(\beta) + f_1 \sin(\omega t + \theta_\beta), & \psi_8 &= -f_0 \sin(\beta) + f_1 \sin(\omega t + \theta_\beta), \end{aligned} \quad (4.11)$$

where α , β and θ_β are constant and arbitrary phase(though those phases are not important due to gauge symmetry). Under such a setup, take those for ψ_1 as an example among eight. The equation of motion of ψ_1 can then be rearranged by substituting by f_0 and f_1 as

$$0 = -\frac{d^2}{dt^2}(f_0 \cos(\alpha) + f_1 \cos(\omega t)) + \nabla^2(f_0 \cos(\alpha) + f_1 \cos(\omega t)) + \mu(f_0 \cos(\alpha) + f_1 \cos(\omega t)) - 4\lambda(f_0 \cos(\alpha) + f_1 \cos(\omega t))(2f_0^2 + 2f_1^2) - 4\lambda_4(-f_0 \cos(\alpha) + f_1 \cos(\omega t))(-f_0^2 + f_1^2), \quad (4.12)$$

where all other phase parameters are canceled in trigonometric. Then we can repeat separating terms based on frequency spectrum step as we did in the 4-field system, and we will end up with another equation set that describes the shape of f_0 and f_1 .

$$\begin{aligned} 0 &= \nabla^2 f_0 + \mu f_0 - 4\lambda f_0(2f_0^2 + 2f_1^2) + 4\lambda_4 f_0(-f_0^2 + f_1^2), \\ 0 &= \omega^2 f_1 + \nabla^2 f_1 + \mu f_1 - 4\lambda f_1(2f_0^2 + 2f_1^2) - 4\lambda_4 f_1(-f_0^2 + f_1^2). \end{aligned} \quad (4.13)$$

Like the theory of the 4-field system, the system is valid without any radiation; that is, the solution lasts forever. Derivation of any other seven fields gives the same results. Plots of f_0 and f_1 are given in FIG. 6, and they follow almost the same pattern as previously discussed in the 4-field system.

After finishing the 2HDM setup, we repeat the Floquet analysis of stability to compare it with the 4-field system. As shown in the FIG. 7, like in the 4-field system, Floquet analysis also confirms the linear stability. FIG. 7 further shows that there is a greater proportion of modes with $|\rho| < 1$ in 2HDM than in the 4-field system, indicating systems are more likely to converge when under random perturbation(faster in self-correlation), consistent with the outcomes of FIG. 2 where 2HDM bubbles have average longer lifetimes than the 4-field system.

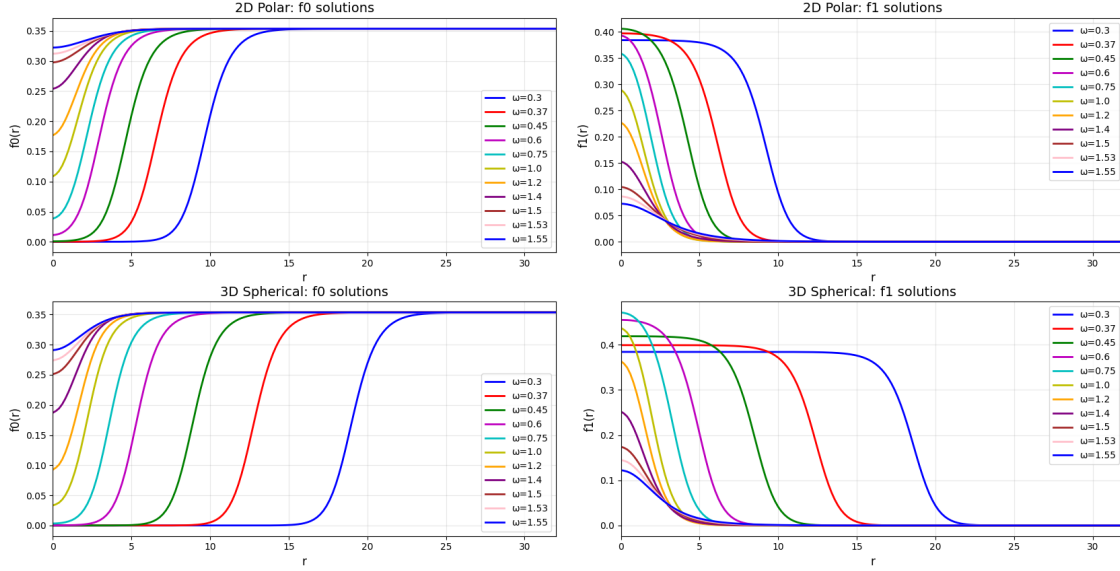


FIG. 6. 2HDM plot of f_0 and f_1 , in 2D and 3D space, under the parameter chosen from Appendix 1 with full mixing. Those functions follow the same pattern as we discussed in the 4-field system, but with generally lower amplitudes.

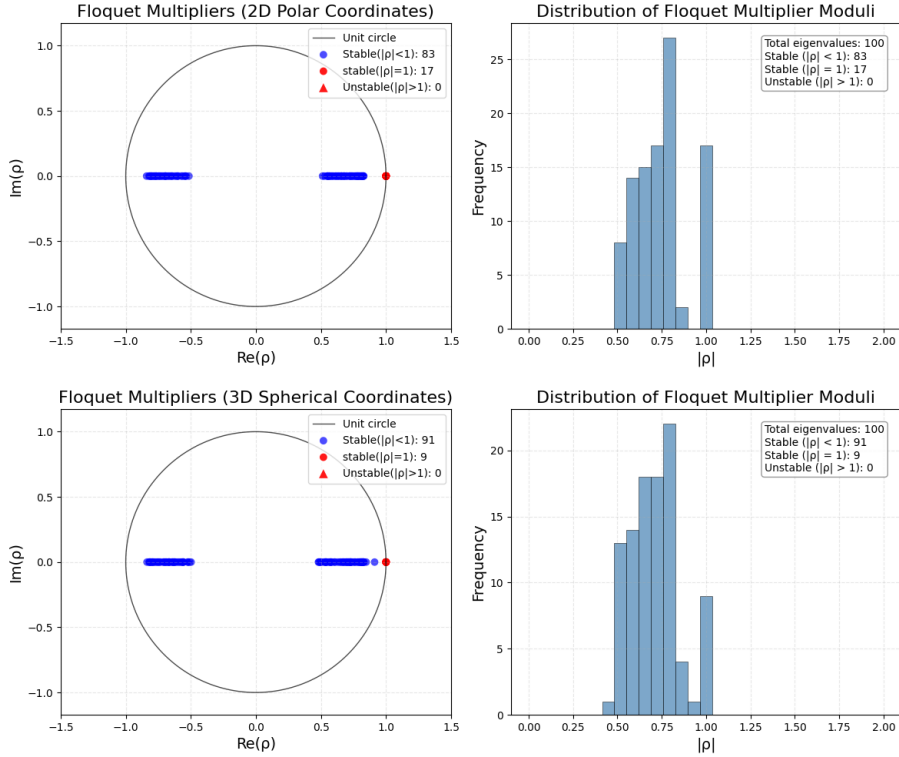


FIG. 7. Repeat of Floquet in 2HDM, with background solution is taken when $\omega = 0.45$ as an example, and $\alpha = \beta = \pi/4$, and $\theta_\beta = 0$. Other parameters from Appendix 1 with full mixing. Like in analysis in 4-field system, further plots show the system is stable under any ω in range.

V. CONCLUSION

From the unexpected decay curve of the system starting with random initial conditions in previous research, we observe an oscillatory solution that exists as a long-lived, bubble-like closed domain wall, and such a structure has been reproduced successfully in the artificial setup in 4-field theory as well as in 2HDM, with oscillating in one vacuum manifold inside and stationary at another vacuum outside.

We also found that, when under some special choice in parameter space, the structure becomes an Exact Oscillon, which is radiation-free, and its lifetime is expected to reach infinity. The computer modeling results are consistent with our predictions. However, while the mathematical stability is demonstrated, the precise topological protection mechanism warrants further investigation. which will be the subject of future work. Besides, even if the theories are highly suppressed in modern cosmology due to restrictions in parameters, such a mathematical structure could be applicable somewhere in condensed matter physics, where interaction parameters could be manually adjusted to fit the requirement.

There are also some limitations of using classical wave motion to simulate quantum field theories, though mechanics share some similarities, but there are still some differences between them. Our classical field simulation can be used as a reference, but be aware that it might be different from realistic physical behaviors.

ACKNOWLEDGMENTS

I would like to express my thanks to Prof. Zhaofeng Kang for his enthusiastic support and invaluable guidance throughout this research, and to Prof. Kecheng Wang and Prof. Yinnan Mao for their help in improving cosmology background knowledge.

I am also grateful to Prof. Richard A. Battye and Dr. Steven J. Cotterill for their guidance and supervision in my master's research project, which is the former version of this research.

-
- [1] H. M. Hodges, "Domain walls with bound bose condensates," *Phys. Rev. D*, vol. 37, pp. 3052–3055, May 1988. [Online]. Available: <https://link.aps.org/doi/10.1103/PhysRevD.37.3052>
 - [2] T. W. B. Kibble, "Topology of cosmic domains and strings," *Journal of Physics A: Mathematical and General*, vol. 9, no. 8, p. 1387, aug 1976. [Online]. Available:

- <https://dx.doi.org/10.1088/0305-4470/9/8/029>
- [3] Y. B. Zeldovich, I. Y. Kobzarev, and L. B. Okun, “Cosmological Consequences of the Spontaneous Breakdown of Discrete Symmetry,” *Zh. Eksp. Teor. Fiz.*, vol. 67, pp. 3–11, 1974.
 - [4] R. A. Battye, A. Pilaftsis, and D. G. Viatic, “Domain wall constraints on two-Higgs-doublet models with Z_2 symmetry,” *Phys. Rev. D*, vol. 102, no. 12, p. 123536, 2020.
 - [5] A. Vilenkin and E. P. S. Shellard, *Cosmic strings and other topological defects*, ser. Cambridge monographs on mathematical physics. Cambridge: Cambridge University Press, 1994.
 - [6] J. N. Benabou, M. Buschmann, S. Kumar, Y. Park, and B. R. Safdi, “Signatures of primordial energy injection from axion strings,” p. 055005, Mar 2024. [Online]. Available: <https://link.aps.org/doi/10.1103/PhysRevD.109.055005>
 - [7] A. Vilenkin and A. E. Everett, “Cosmic strings and domain walls in models with goldstone and pseudo-goldstone bosons,” *Phys. Rev. Lett.*, vol. 48, pp. 1867–1870, Jun 1982. [Online]. Available: <https://link.aps.org/doi/10.1103/PhysRevLett.48.1867>
 - [8] N. Kitajima, “Primordial black hole formation from collapsing domain walls with full general relativity,” 2025. [Online]. Available: <https://arxiv.org/abs/2510.22759>
 - [9] G. Dvali, Z. Tavartkiladze, and J. Nanobashvili, “Biased discrete symmetry and domain wall problem,” *Physics Letters B*, vol. 352, no. 3–4, p. 214–219, Jun. 1995. [Online]. Available: [http://dx.doi.org/10.1016/0370-2693\(95\)00511-I](http://dx.doi.org/10.1016/0370-2693(95)00511-I)
 - [10] R. A. Battye, S. J. Cotterill, E. S. Andres, and A. K. Thomasson, “Percolation of domain walls in the two-higgs doublet model,” *Physics Letters B*, vol. 862, p. 139311, 2025. [Online]. Available: <https://www.sciencedirect.com/science/article/pii/S0370269325000711>
 - [11] R. A. Battye, S. J. Cotterill, and P. Millington, “Vortex stability in pseudo-Hermitian theories,” 11 2025.
 - [12] S. Gabriel and S. Nandi, “A new two higgs doublet model,” *Physics Letters B*, vol. 655, no. 3, pp. 141–147, 2007. [Online]. Available: <https://www.sciencedirect.com/science/article/pii/S0370269307005473>
 - [13] R. A. Battye, G. D. Brawn, and A. Pilaftsis, “Vacuum topology of the two higgs doublet model,” *Journal of High Energy Physics*, vol. 2011, no. 8, Aug. 2011. [Online]. Available: [http://dx.doi.org/10.1007/JHEP08\(2011\)020](http://dx.doi.org/10.1007/JHEP08(2011)020)
 - [14] R. A. Battye and S. J. Cotterill, “Spontaneous hopf fibration in the two-higgs-doublet model,” p. 061601, Feb 2024. [Online]. Available: <https://link.aps.org/doi/10.1103/PhysRevLett.132.061601>
 - [15] G. Branco, P. Ferreira, L. Lavoura, M. Rebelo, M. Sher, and J. P. Silva, “Theory and phenomenology of two-higgs-doublet models,” *Physics Reports*, vol. 516, no. 1, pp. 1–102, 2012, theory and phenomenology of two-Higgs-doublet models. [Online]. Available:

<https://www.sciencedirect.com/science/article/pii/S0370157312000695>

- [16] N. Darvishi, A. Pilaftsis, and J.-H. Yu, “Maximising cp violation in naturally aligned two-higgs doublet models,” *Journal of High Energy Physics*, vol. 2024, no. 5, May 2024. [Online]. Available: [http://dx.doi.org/10.1007/JHEP05\(2024\)233](http://dx.doi.org/10.1007/JHEP05(2024)233)
- [17] J.-O. Gong, H. M. Lee, and S. K. Kang, “Inflation and dark matter in two higgs doublet models,” *Journal of High Energy Physics*, vol. 2012, no. 4, Apr. 2012. [Online]. Available: [http://dx.doi.org/10.1007/JHEP04\(2012\)128](http://dx.doi.org/10.1007/JHEP04(2012)128)
- [18] R. A. Battye, A. Pilaftsis, and D. G. Viatic, “Simulations of domain walls in two higgs doublet models,” *Journal of High Energy Physics*, vol. 2021, no. 1, Jan. 2021. [Online]. Available: [http://dx.doi.org/10.1007/JHEP01\(2021\)105](http://dx.doi.org/10.1007/JHEP01(2021)105)
- [19] I. P. Ivanov, “Erratum: Minkowski space structure of the higgs potential in the two-higgs-doublet model [phys. rev. d 75, 035001 (2007)],” *Phys. Rev. D*, vol. 76, p. 039902, Aug 2007. [Online]. Available: <https://link.aps.org/doi/10.1103/PhysRevD.76.039902>
- [20] D. Wang and S. Dong, “A discussion of numerical wave absorption using sponge layer methods,” *Ocean Engineering*, vol. 247, p. 110732, 2022. [Online]. Available: <https://www.sciencedirect.com/science/article/pii/S0029801822001834>
- [21] G. Mur, “Absorbing boundary conditions for the finite-difference approximation of the time-domain electromagnetic-field equations,” *IEEE Transactions on Electromagnetic Compatibility*, vol. EMC-23, no. 4, pp. 377–382, 1981.
- [22] M. A. Amin and D. Shirokoff, “Flat-top oscillons in an expanding universe,” *Physical Review D*, vol. 81, no. 8, Apr. 2010. [Online]. Available: <http://dx.doi.org/10.1103/PhysRevD.81.085045>
- [23] P. Salmi and M. Hindmarsh, “Radiation and Relaxation of Oscillons,” *Phys. Rev. D*, vol. 85, p. 085033, 2012.
- [24] B. Hespel, D. López-Val, and E. Vryonidou, “Higgs pair production via gluon fusion in the two-higgs-doublet model,” *Journal of High Energy Physics*, vol. 2014, no. 9, Sep. 2014. [Online]. Available: [http://dx.doi.org/10.1007/JHEP09\(2014\)124](http://dx.doi.org/10.1007/JHEP09(2014)124)

APPENDIX 1: 2HDM MASS AND PARAMETERS

From previous research, the values of μ and λ can be expressed in the form of the values of the mass of particles and mixing angles [4, 19, 24],

$$\mu_1 = \frac{M_h^2 \cos(a)^2 + M_H^2 \sin(a)^2 + (M_h^2 - M_H^2) \cos(a) \sin(a) \tan(b)}{2M_h^2}, \quad (5.1)$$

$$\mu_2 = \frac{M_h^2 \cos(a)^2 + M_H^2 \sin(a)^2 + (M_h^2 - M_H^2) \cos(a) \sin(a) \cot(b)}{2M_h^2}, \quad (5.2)$$

$$\lambda_1 = \frac{M_h^2 \cos(a)^2 + M_H^2 \sin(a)^2}{2M_h^2 \cos(b)^2}, \quad (5.3)$$

$$\lambda_2 = \frac{M_h^2 \sin(a)^2 + M_H^2 \cos(a)^2}{2M_h^2 \sin(b)^2}, \quad (5.4)$$

$$\lambda_3 = \frac{(M_h^2 - M_H^2) \cos(a) \sin(a) + 2M_{H\pm}^2 \cos(b) \sin(b)}{M_h^2 \cos(b) \sin(b)}, \quad (5.5)$$

$$\lambda_4 = \frac{M_A^2 - 2M_{H\pm}^2}{M_h^2}, \quad (5.6)$$

$$\lambda_5 = \frac{M_A^2}{M_h^2}, \quad (5.7)$$

with normalized by the original Higgs boson mass $M_h = 125\text{GeV}$, and given v_1 and v_2 can be expressed as [18]

$$v_1 = \cos(b)v_{\text{SM}}, \quad v_2 = \sin(b)v_{\text{SM}} \quad (5.8)$$

and vacuum expectation value v_{SM} is measured to be 246GeV . Other values remain set to be: $M_H = M_A = M_{H\pm} = 200\text{GeV}$ [4] for making the calculation simpler and easier.

In the early random trial of section III, we choose Mixing Angle parameter $\tan(a) = \tan(b) = 0.85$ [4], and after we found the radiation-free condition requires $a = b = \pi/4$ (full mixing). Parameters in radiation-free condition gives $\mu_1 = \mu_2 = 0.5$, $\lambda_1 = \lambda_2 = 1.78$, $\lambda_3 = 3.56$, $\lambda_4 = -2.56$, and $\lambda_5 = 2.56$.

All parameters have been averaged using terms of M_h so they are dimensionless. If we want to transfer any values back to SI units, just multiply them by M_h mass values.

APPENDIX 2: PARAMETER AND MASS IN 4-FIELD SYSTEM

After reducing 4 degrees of freedom, the 4-field system predict predict less particle than in 2HDM.

The Lagrangian density can be written in terms of tensors of

$$\mathcal{L} = (\partial_\mu \Psi_i)(\partial^\mu \Psi_i) - V(\underline{\Psi}), \quad (5.9)$$

where array of fields $\underline{\Psi}$ decompose into its elements Ψ_i , the Lagrangian is invariant under symmetrical group transformation

$$\Psi_i \rightarrow \Psi'_i = \Psi_i + i\theta^a T_{ij}^a \Psi_j, \quad (5.10)$$

for lie group generator T^a with elements in its matrix representation T_{ij}^a , of Lie-group $G = SO(n)$ of n dimensional(number of fields) used, with infinitesimal change θ^a .

Since potential $V(\underline{\Psi})$ invariant under this transformation, $\delta V = V(\Psi) - V(\Psi') = 0$, so $\delta V = i\theta^a T_{ij}^a \Psi_j = 0$, which further gives $T_{ij}^a \Psi_j = 0$.

Then Taylor expand $\underline{\Psi}$ around a vacuum solution \underline{v} by $\underline{\Psi} = \underline{v} + \underline{\psi}$, as the first order term is zero as $T_{ij}^a \Psi_j = 0$, the expansion is

$$V(\underline{\Psi}) = V(\underline{v}) + \frac{1}{2} M_{ij}^2 \psi_i \psi_j + \mathcal{O}, \quad (5.11)$$

where

$$M_{ij}^2 = \left. \frac{\partial^2 V}{\partial \Psi_i \partial \Psi_j} \right|_{\underline{\Psi}=\underline{v}}, \quad (5.12)$$

and M_{ij}^2 is called the mass matrix of fields ψ_i .

By choosing the following fields basis

$$\Psi_1 = v + \psi_1 + ia_1 \quad \text{and} \quad \Psi_2 = v + \psi_2 + ia_2, \quad (5.13)$$

With scalar fields ψ_1, ψ_2, a_1, a_2 and vacuum $v = f_0 = \sqrt{\frac{\mu^2}{4\lambda + 2\lambda_4}}$. Using the total potential can be expended into

$$\begin{aligned} V(\Psi_1, \Psi_2) = & -\mu^2((v + \psi_1)^2 + a_1^2) - \mu^2((v + \psi_2)^2 + a_2^2) + \lambda((v + \psi_1)^2 + a_1^2)^2 + \lambda((v + \psi_2)^2 + a_2^2)^2 \\ & + 2\lambda((v + \psi_1)^2 + a_1^2)((v + \psi_2)^2 + a_2^2) + 2\lambda_4 [(v + \psi_1)(v + \psi_1) + a_1 a_2]^2, \end{aligned} \quad (5.14)$$

where their corresponding part in the matrix can be extracted and separated into several parts without crossing each other. Those sectors can be expressed as

$$M_{h,H}^2 = \frac{1}{2} \frac{\partial^2 V}{\partial \psi_i \partial \psi_j} = \begin{pmatrix} 4\lambda v^2 & 4(\lambda + \lambda_4)v^2 \\ 4(\lambda + \lambda_4)v^2 & 4\lambda v^2 \end{pmatrix}, \quad (5.15)$$

$$M_A^2 = \frac{1}{2} \frac{\partial^2 V}{\partial a_i \partial a_j} = -2\lambda_4 \begin{pmatrix} v^2 & -v^2 \\ -v^2 & v^2 \end{pmatrix}, \quad (5.16)$$

The actual mass values are the eigenvalues of those matrices, which are:

$$m_H^2 = M_A^2 = \frac{-2\lambda_4}{2\lambda + \lambda_4} \mu^2, \quad m_h^2 = 2\mu^2, \quad m_G^2 = 0. \quad (5.17)$$

with one massless Goldstone boson and a pair of degenerate particles with opposite parity. Therefore, for the sake of vacuum stability, one requires the following

$$\lambda > 0, \quad 0 > \lambda_4 > -2\lambda. \quad (5.18)$$

like in Appendix 2, we take $m_h = 1$ and let every parameter be averaged by it, then we use $\mu = 0.5$, $\lambda = 1.78$, and $\lambda_4 = -2.56$ for parameter in the analysis of this paper.

APPENDIX 3: FLOQUET ANALYSIS

In the framework of Floquet theory, a perturbation function δ_{ψ_i} is introduced for each of the four fields. The linearized equation of motion takes the form

$$\ddot{\delta}_i = \hat{D}\delta_i + \hat{J}(t)_{ij}\delta_j, \quad (5.19)$$

we may define State Vector $\vec{v} = (\dot{\delta}_i, \delta_i)^T$ and the stability matrix of evolution

$$A = \begin{pmatrix} 0 & \hat{\mathbb{I}} \\ \hat{D} + \hat{J} & 0 \end{pmatrix}, \quad (5.20)$$

so that $\dot{\vec{v}} = A\vec{v}$.

where $\hat{D} = \nabla^2$ is the spatial double differentiation operator matrix and $\hat{J}(t)_{ij} = \frac{\partial^2 V}{\partial \psi_i \partial \psi_j}$ is the Jacobian matrix derived from the potential.

By discretizing the radial coordinate r into a grid of N points with spacing Δr , the system of coupled partial differential equations is transformed into a system of $8N$ ($4N$ for ψ_i and $4N$ for $\dot{\psi}_i$, and $16N$ total in 2HDM) coupled ordinary differential equations. The spatial Laplacian ∇^2 is represented by a tri-diagonal differentiation matrix D , which couples adjacent radial cells.

For the stability matrix that describes the rate of change of the perturbation, we define the Floquet matrix M for describing perturbation change after the evolution over one full oscillation period T , that's $\vec{V}(T) = M\vec{V}(0)$. The Floquet matrix M is described by

$$M = e^{\int_0^T A dt} = \exp \left(\int_0^T \begin{pmatrix} 0 & \hat{\mathbb{I}} \\ \hat{D} + \hat{J} & 0 \end{pmatrix} dt \right), \quad (5.21)$$

where the integration is performed numerically over one period T using discrete time steps $dt \ll T$. If the system needs to achieve a stable configuration over perturbation, the modulus of the matrix eigenvalue should not be greater than 1.